ADVANCED OPTICAL MATERIALS
www.advopticalmat.de

Anomalous Broadband Spectrum Photodetection in 2D Rhenium Disulfide Transistor

Du Xiang, Tao Liu, Junyong Wang, Peng Wang, Lin Wang, Yue Zheng, Yanan Wang, Jing Gao, Kah-Wee Ang, Goki Eda, Weida Hu, Lei Liu, and Wei Chen**

2D transition metal dichalcogenide (TMD)-based phototransistors generally work under photoconductive, photovoltaic, or photogating mode, in which photocarriers are generated from band-to-band excitation. Nevertheless, due to the relatively large bandgap, most TMD phototransistors working under these modes are restricted in visible spectrum. Here, photodetection in 2D multilayer rhenium disulfide (ReS_2) transistor via bolometric mode, which relies on light heating induced conductance change instead of band-to-band photoexcitation is reported, making it possible for sub-bandgap photon detection. The bolometric effect induced photoresponse is first revealed by an anomalous sign switching of photocurrent from positive to negative while increasing gate voltage under visible light, which is further validated by the temperature dependent electrical transport measurements. The phototransistor exhibits remarkable photoresponse under infrared regime, beyond the optical bandgap absorption edge of the ReS_2 flake. Additionally, it demonstrates a low noise equivalent power, less than 5×10^{-2} pW $Hz^{-1/2}$, which is very promising for ultra-weak light detection. Moreover, the response time is below 3 ms, nearly 3–4 orders of magnitude faster than previously reported ReS_2 photodetectors. The findings promise bolometric effect as an effective photodetection mode to extend the response spectrum of large bandgap TMDs for novel and high-performance broadband photodetectors.

1. Introduction

Photodetectors, converting light into electrical signal, demonstrate a wide range of applications in our daily lives, including optical telecommunications, remote sensing, video imaging, motion detection, and so forth.[1–3] 2D layered materials have been rapidly established as promising building blocks for state-of-the-art photodetectors, owing to their unique crystal structure and optical/electrical properties.[4–8] 2D materials possess a layered structure, in which the atoms within each layer are covalently bonded, while different layers are held together by van der Waals interactions. In comparison to the traditional bulk semiconductors, 2D materials demonstrate competitive advantages in the photodetection applications due to their high light absorption efficiency, mechanical flexibility, and convenient processing.[5,6,9–13] Graphene and black phosphorus (BP) have been extensively investigated for broadband photodetectors, which exhibit ultrafast and

Dr. D. Xiang, Dr. T. Liu, Prof. G. Eda, Prof. W. Chen
Department of Chemistry
National University of Singapore
3 Science Drive 3, Singapore 117543, Singapore
E-mail: chmliu@nus.edu.sg; phycw@nus.edu.sg
Dr. D. Xiang, Dr. T. Liu, Dr. J. Wang, Dr. L. Wang, Prof. K.-W. Ang, Prof. G. Eda
Centre for Advanced 2D Materials and Graphene Research Centre
National University of Singapore
6 Science Drive 2, Singapore 117546, Singapore
Dr. J. Wang, Y. Zheng, Y. Wang, J. Gao, Prof. G. Eda, Prof. W. Chen
Department of Physics
National University of Singapore
2 Science Drive 3, Singapore 117542, Singapore
Prof. P. Wang, Prof. W. Hu
State Key Laboratory for Infrared Physics
Shanghai Institute of Technical Physics
Chinese Academy of Sciences
Shanghai 200083, China
The ORCID identification number(s) for the author(s) of this article can be found under https://doi.org/10.1002/adom.201901115.
Prof. K.-W. Ang
Department of Electrical and Computer Engineering
National University of Singapore
4 Engineering Drive 3, Singapore 117583, Singapore
Prof. L. Liu
State Key Laboratory of Luminescence and Applications
Changchun Institute of Optics
Chinese Academy of Sciences
No. 3888 Dongnanhu Road, Changchun 130033, P. R. China
Prof. W. Chen
National University of Singapore (Suzhou) Research Institute
377 Lin Quan Street, Suzhou Industrial Park, Suzhou, Jiangsu 215123, China
Prof. W. Chen
Joint School of National University of Singapore and Tianjin University
International Campus of Tianjin University
Binhai New City, Fuzhou 350207, China

DOI: 10.1002/adom.201901115

wide spectrum photoresponse, arising from their high carrier mobility and small bandgap.[14–22] In addition to graphene and BP, 2D transition metal dichalcogenides (TMDs) based photodetectors have also been intensely studied with superior photoresponsivity and air stability.[5,6,23–25] 2D TMDs photodetectors generally work under photoconductive, photogating or photovoltaic mode, in which the photocarriers are generated from valence band-to-conduction band photoexcitation. However, due to the relatively large bandgap, the investigations of most TMDs photodetectors under the above modes are restricted in visible spectrum. To extend the detection window of large bandgap TMDs, the discovery of other photoresponse modes is highly desirable. Bolometric effect, another photodetection mode, is associated with the transport conductance change in temperature-sensitive materials due to photon absorption-induced heating.[5,6] Since bolometric effect does not rely on band-to-band photoexcitation, it may induce sub-bandgap photon detection in TMDs, and greatly broaden their photoresponse spectrum. Bolometric effect has been investigated in graphene and BP, whereas it is seldom observed in TMDs.[14,19,26]

Rhenium disulfide (ReS_2), as a fast emerging 2D TMD, has drawn special attention due to its extraordinary electrical/optical properties.[27–33] In contrast to other TMDs, ReS_2 maintains a direct bandgap (≈1.5 to 1.6 eV), originating from its weak interlayer coupling, which is very promising for optoelectronic applications.[31–33] Moreover, the distorted T phase structure enables the detection of polarized optical signal in ReS_2 photodetectors.[31,32] In this work, we report bolometric effect induced fast and anisotropic photodetection in 2D multilayer rhenium disulfide (ReS_2) transistor with visible-to-infrared sensitivity, in which the polarity of photoresponse can be tuned by backgate. The response time (<3 ms) is 3–4 orders of magnitude faster than the previously reported ReS_2 photodetectors. This bolometric effect driven photoresponse mode is further validated by temperature dependent electrical transport measurements. As expected, our phototransistor exhibits remarkable photoresponse under infrared illumination (wavelength from 900 to 1200 nm), beyond the optical bandgap absorption edge of ReS_2 (optical bandgap ≈1.525 eV). Additionally, it demonstrates a noise equivalent power below 5×10^{-2} pW $Hz^{-1/2}$, indicating its great potential for ultralow light power detection.

2. Results and Discussion

Figure 1a,b (inset) shows the schematic and optical image of the ReS_2 photodetector fabricated in a field-effect-transistor configuration. The detail for sample preparation and device

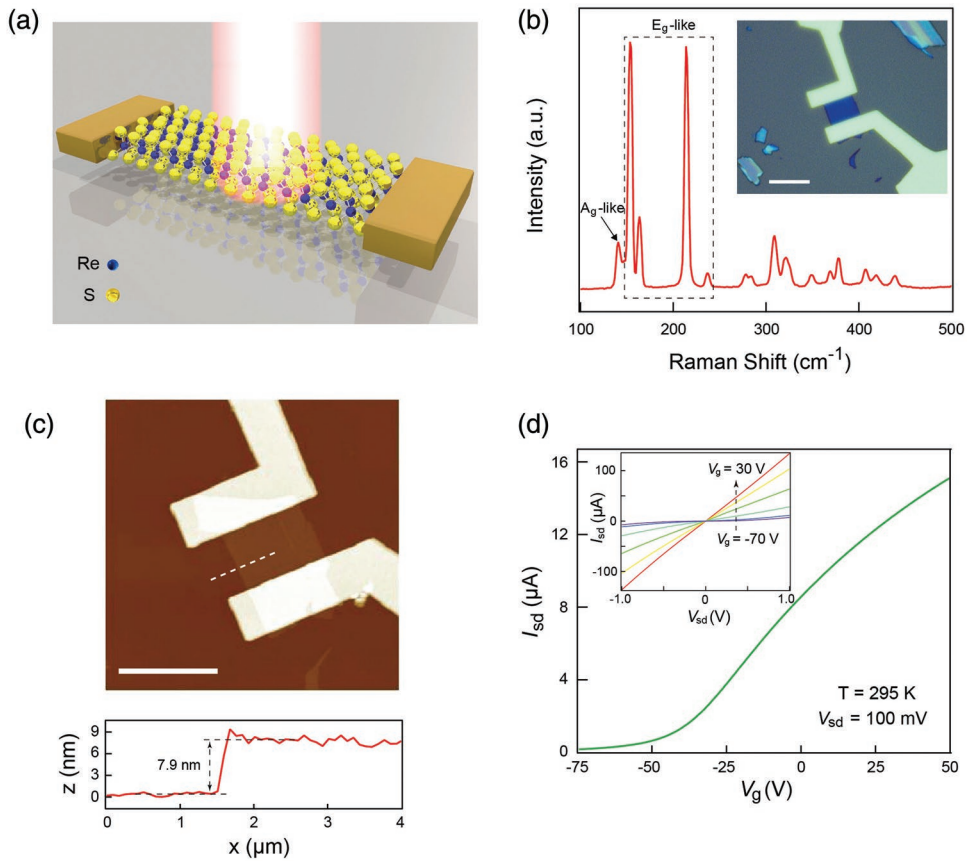

Figure 1. a) Schematic illustration of the ReS_2 phototransistor fabricated on SiO_2/Si substrate. b) Raman spectrum of ReS_2 crystal, with two characteristic modes, A_g-like and E_g-like modes. Inset is the optical image of the as-fabricated ReS_2 device. Scale bar is 5 μm. c) AFM image of the same device. Scale bar is 5 μm. The AFM line profile reveals the thickness of ReS_2 flake, around ≈7.9 nm, that is, ≈10 atomic layers. d) Transfer and output (inset) curves of the device at $T = 295$ K. The output curves were obtained at different V_g from −70 to 30 V with 20 V step.

fabrication is demonstrated in the Experimental Section. The 2D ReS_2 crystals were confirmed by Raman spectroscopy (Figure 1b). The characteristic peak located at 140.7 cm^{-1} corresponds to the A_g-like modes, due to the out-of-plane vibrations of Re atoms.[34] The four peaks located at 154.7, 163.5, 215.0, and 237.5 cm^{-1} can be assigned to the E_g-like modes, ascribing to the in-plane vibrations of Re atoms. The rest Raman peaks at higher frequency originate from the vibrations of S atoms. The AFM characterization (shown in Figure 1c) reveals the thickness of the ReS_2 flake. The flake thickness is around ≈7.9 nm, that is, ≈10 atomic layers. Figure 1d exhibits the transfer and output characteristics of the ReS_2 device. The transistor demonstrates typical n-type transport behavior while sweeping the gate voltage V_g from −75 to 50 V. The filed-effect electron mobility (μ) can be extracted from the transfer curve by using the equation

$$\mu = \frac{L}{WC_iV_{sd}}\frac{dI_{sd}}{dV_g} \quad (1)$$

where C_i is the capacitance per unit area of 300 nm SiO_2. L and W are the length and width of conduction channel, respectively. The electron mobility is estimated around 50 $cm^2\ V^{-1}\ s^{-1}$, which is consistent with previous reports.[32]

We then characterized the photoresponse of the ReS_2 phototransistor. **Figure 2**a,b shows the time dependent photoresponse of the ReS_2 phototransistor at two different

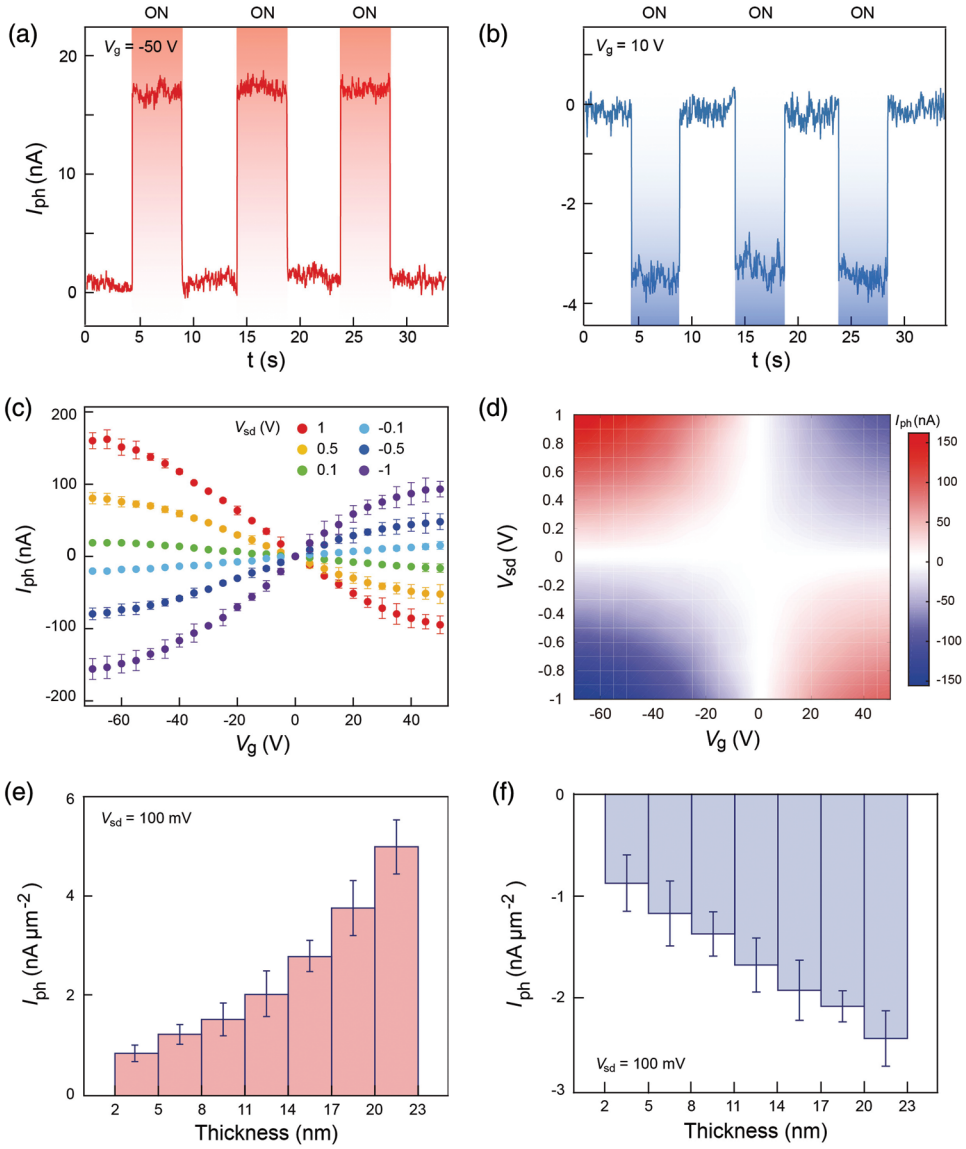

Figure 2. Time dependent photoresponse of the transistor under V_g = a) −50 V and b) 10 V. The bias and illumination condition are fixed for these two measurements, where V_{sd} = 0.1 V, wavelength λ = 638 nm. c) Photocurrent versus gate voltage at different biases (V_{sd} from −1 to 1 V). The photocurrent changes its polarity from positive to negative at around V_g = 0 V, applicable to all the biases. d) 2D mapping of the photocurrent as a function of gate and bias voltages, which presents a clearer picture of the polarity switching of the photocurrent. Maximum e) positive and f) negative photocurrent density of each ReS_2 phototransistor are statistically summarized as a function of flake thickness from 2 to 23 nm. Both the positive and negative photocurrents are gradually improved with increasing the thickness.

backgates V_g = −50 and 10 V, under the same bias (V_{sd} = 0.1 V) and light illumination condition (λ = 638 nm). Here the photocurrent (I_{ph}) is defined as: $I_{ph} = I_{light} - I_{dark}$, where I_{light} and I_{dark} are the source–drain current under light illumination and dark condition, respectively. Interestingly, we observed opposite polarity of the photocurrent, which is positive at V_g = −50 V, and becomes negative when V_g is changed to 10 V. Such gate-controlled polarity change of I_{ph} is also observed at other visible lights (λ = 515 and 473 nm), as shown in Figure S1 of the Supporting Information, which is consistent with the phenomenon at 638 nm. To further illustrate the anomalous photodetection behavior of the ReS_2 transistor, we investigated the I_{ph} at various V_g and V_{sd}, as plotted in Figure 2c,d. The polarity switching of I_{ph} occurs at around V_g = 0 V, applicable for all bias conditions from −1 to 1 V. Note that this device with sharp switching point at V_g = 0 V is one of the representative devices. Other devices, in a statistical manner, possess sample-to-sample variation in their switching points (Figure S2, Supporting Information). Additionally, the photocurrent exhibits similar trend when increasing V_g in both positive and negative directions. To further validate our observations and exclude the statistical outliers, we fabricated 50 ReS_2 transistors with various thicknesses (2 to 23 nm) and studied their photoresponse behavior under the same condition. All the devices demonstrate gate tunable positive and negative photocurrent, with device-to-device variation of the crossover gate voltage. Figure 2e,f shows the statistics of the maximum positive and negative photocurrent density of each ReS_2 phototransistor as a function of flake thickness. As the thickness increases from 2 to 23 nm, the positive I_{ph} is gradually enhanced by nearly five times. Likewise, the negative I_{ph} is progressively increased by around three times when the thickness reaches up to 23 nm. We also investigated the stability of the ReS_2 phototransistor, as shown in Figure S3 of the Supporting Information. The electrical transport behavior and photocurrent of the device are nearly maintained after storage in ambient condition for three months, indicating its excellent air stability.

2D TMDs based phototransistors generally show positive photocurrent under visible light illumination, in regardless of different doping levels modulated either by external electric field or physical/chemical decoration. The positive photoresponse is mainly due to the generation and transport of photo-excited carriers in TMD transistors. Intriguingly, we observed both positive and negative photoresponse in our ReS_2 transistors controlled by the backgate in the visible light regime, a photodetection behavior which is distinct from other reported TMDs phototransistors. Previous studies in graphene and BP photodetectors propose that the negative photoresponse in their devices originates from light irradiation induced thermal effect, including photothermoelectric (PTE) effect (Seebeck effect) and bolometric effect.[14,19] The PTE effect originates from the temperature gradient in the 2D channel by local light illumination, while the bolometric effect is due to the change of transport conductance of the material under light heating. In our photoresponse measurements, the spot size of xenon light is around 20 mm^2, six orders of magnitude larger than the size of the ReS_2 device. Hence, we assume uniform illumination on the device and neglect the temperature gradient induced PTE effect. Moreover, the photocurrent generated by PTE effect is self-driven since the photogenerated hot electrons can produce a photovoltage across the device. By contrast, without applying an external bias on the device, the photocurrent induced by bolometric effect cannot be observed. Therefore, we then investigated the photoresponse of the ReS_2 device under different biases, as shown in **Figure 3**a. There is no photocurrent emerging at V_{sd} = 0 V, indicating the negligible PTE effect in ReS_2 device under illumination, which is consistent with our hypothesis. On the other hand, the photocurrent increases almost linearly with increasing V_{sd} from 0.1 to 1 V, in good agreement with the photocurrent trend induced by bolometric effect in BP photodetector.[19] These results indicate bolometric effect as the dominating mechanism for the negative photocurrent in our ReS_2 devices.

To further reveal the underlying bolometric effect, we investigated the temperature dependent electrical transport property of the ReS_2 transistor shown in Figure 2. As the temperature decreases from 290 to 80 K, a metal–insulator transition (MIT) with cross-over point at around V_g = 0 V is clearly observed (Figure 3b). This is consistent with the gate-controlled sign switching of the photocurrent shown in Figure 2, since the bolometric coefficient has opposite sign in semiconducting phase and metallic phase. From Figure 3b, we extract the gate dependent bolometric coefficient β which describes the sensitivity of the transport current I to the change of temperature T around room temperature (T_0 = 295 K). β is calculated by the equation: $\beta(V_g) = \Delta I(V_g)/\Delta T(V_g)$, and plotted as a function of gate voltage in Figure 3c. The β is negative in the positive gate regime, and keeps declining with increasing the V_g, which is in good agreement with the I_{ph} trend as shown in the inset of Figure 3c. This further validates that the bolometric effect dominates the negative I_{ph}, as illustrated by the energy band diagram in Figure 3e. By contrast, when V_g is negative, the β switches to positive. The β reaches its maximum at around V_g = −30 V, followed by a gradual decay when further increasing V_g to −70 V. The rising trend in β (V_g = 0 V to −30 V) resembles the photocurrent curve as shown in the inset of Figure 3c, whereas the photoresponse behavior from V_g = −30 to −70 V cannot be clarified by only considering the bolometric effect. We propose that the increase of positive I_{ph} in this regime (V_g = −30 to −70 V) originates from the photovoltaic effect, which becomes predominant due to the increase of Schottky barrier between ReS_2 and metal contact (Figure S4, Supporting Information). To further confirm the crossover from bolometric effect to photovoltaic effect, we calculated the gate dependent activation energy E_A from the Arrhenius plot by the equation $G \approx \exp(E_A/K_BT)$ (Figure 3d), where G is the conductance, K_B is the Boltzmann constant. As V_g increases from −30 to −70 V, the linearity between E_A and V_g is gradually improved, illustrating the enhancement of Schottky barrier,[35] which leads to more significant photovoltaic effect. These results are consistent with the improvement of I_{pv} (photocurrent induced by photovoltaic effect) at V_g beyond −30 V. The schematic in Figure 3f demonstrates that the positive I_{ph} is contributed by both the bolometric and photovoltaic effect in the negative gate regime.

The bandgap of ReS_2 crystal ranges from 1.5 to 1.6 eV depending on its thickness.[31–33] Such large bandgap restricts its application in infrared photodetectors for the case that the photoresponse relies on traditional band-to-band photoexcitation.

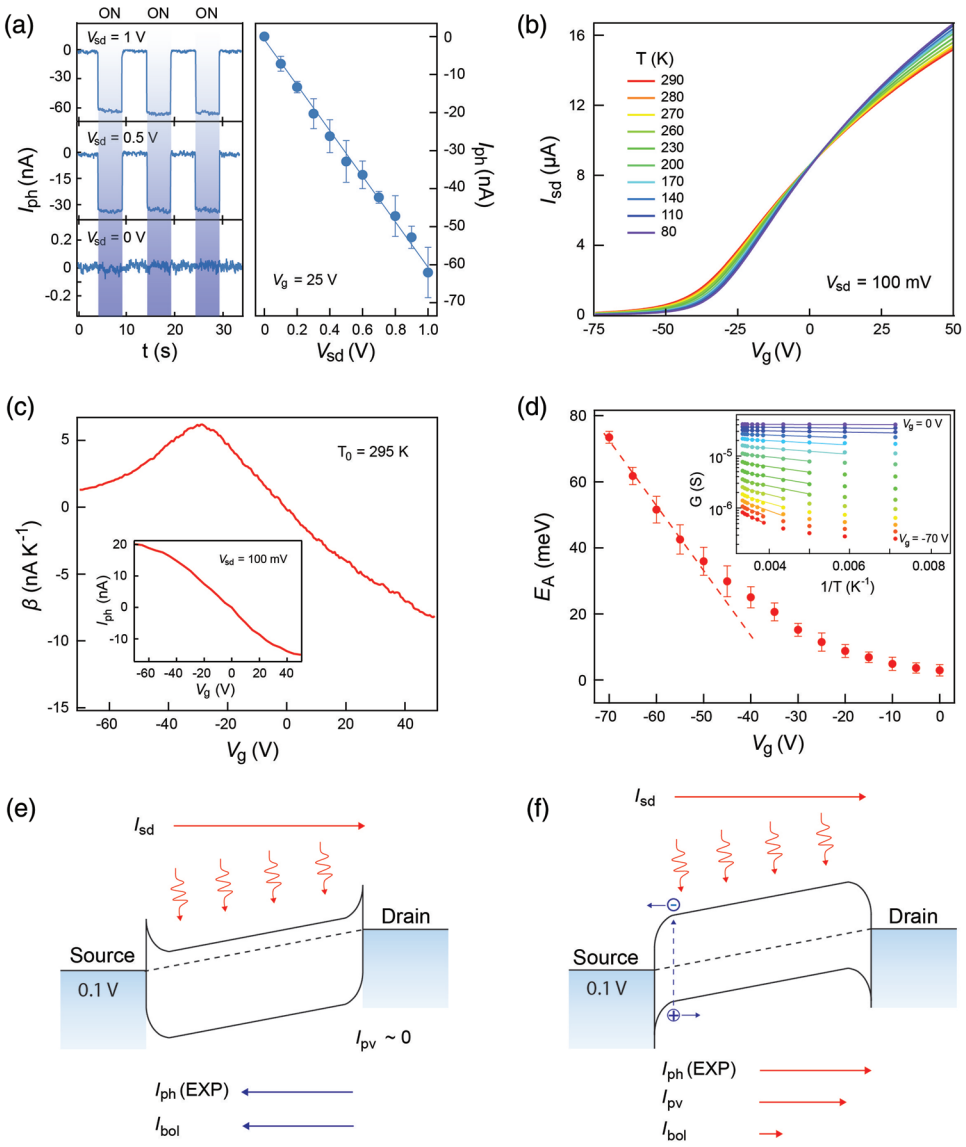

Figure 3. a) Bias dependent photocurrent under V_g = 25 V. The V_{sd} increases from 0 to 1 V. There is no detectable photoresponse at zero bias, while the photocurrent increases almost linearly with increasing V_{sd} from 0.1 to 1 V. b) Temperature dependent transport measurement of the ReS_2 transistor. A metal–insulator transition with crossover point at around V_g = 0 V is clearly observed. c) Gate dependent bolometric coefficient at T_0 = 295 K. Inset is the experimentally measured total photocurrent. The trend of total I_{ph} is well described by adding up bolometric and photovoltaic effects. d) The extracted activation energy as a function of gate voltage. Inset is the Arrhenius plot of conductance (G). The activation energy (E_A) shows a gradual evolution from gate independent tunneling to gate dependent thermionic emission with increasing V_g from –20 to –50 V. The energy band diagram in e) bolometric-dominated and f) photovoltaic-dominated regimes demonstrate the polarity of experimentally measured photocurrent. I_{bol} and I_{pv} represent the photocurrent induced by bolometric effect and photovoltaic effect, respectively.

Bolometric effect induced photoresponse has been observed over the visible spectrum in the ReS_2 transistor, which sheds light for the application of ReS_2 in infrared photodetection. Therefore, we investigated the photoresponse of ReS_2 transistor in the infrared regime beyond its bandgap. To confirm the optical bandgap of few-layer ReS_2, we studied the absorption spectrum of few-layer ReS_2 flake on quartz substrate (**Figure 4**a). To ensure the bandgap consistency, the thickness of the selected ReS_2 flake for absorption measurement is ≈7.65 nm (Figure S5a, Supporting Information), very approximating to that of the ReS_2 device (≈7.9 nm) for photodetection measurement. An excitonic peak located at ≈813 nm is clearly identified in the spectrum, which is consistent with the PL peak at ≈1.525 eV (Figures S5b and S6, Supporting Information). These results suggest that the optical bandgap of the ReS_2 flake is around ≈1.525 eV, in good agreement with previous reports.[31–33] To qualitatively investigate the possibility of gap states induced photoresponse at lower energy, we measured the PL spectra of ReS_2 flake from 500 to 2200 nm at both T = 300 K and T = 77 K (Figure S7, Supporting Information). We did not observe any exciton peak from 1000 nm onward in both spectra, indicating the minor impact of gap states in the photoresponse within the wavelength range covered in our experiments.

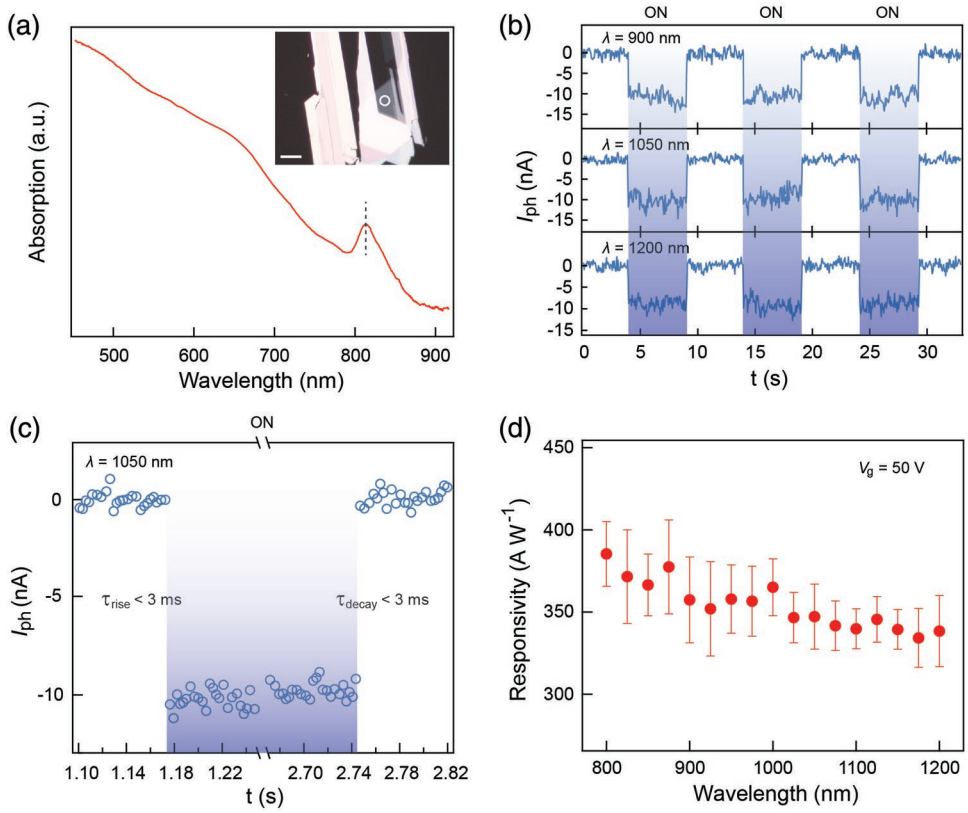

Figure 4. a) Absorption spectrum of ReS_2 flake. Inset: optical image of the ReS_2 flake for the absorption spectrum measurement on quartz substrate. The white circle in the optical image indicates the region for measurement. The scale bar is 5 µm. b) Time dependent photoresponse of the transistor at three different infrared wavelengths (λ = 900, 1050, and 1200 nm). The power is around 50 µW for the three lights. The gate and bias are fixed for each measurement, V_g = 50 V and V_{sd} = 0.1 V. Note that all the three wavelengths are beyond the optical bandgap absorption edge of the ReS_2 flake. c) Measurement of the photoresponse time at λ = 1050 nm. Both the rising and decaying time are less than 3 ms, exceeding the highest accuracy of our electrical measurement unit. d) Photoresponsivity versus wavelength at V_g = 50 V and V_{sd} = 0.1 V. The wavelength ranges from 800 to 1200 nm.

Figure 4b demonstrates time dependent photoresponse of the ReS_2 device under three infrared lights at V_g = 50 V, V_{sd} = 0.1 V. Note that the xenon lamp in our setup can only provide lights with wavelength from 350 to 1200 nm. Nevertheless, the wavelengths of the three selected infrared lights (λ = ≈900, 1050, and 1200 nm) are all beyond the optical bandgap absorption edge of the ReS_2 flake (λ = ≈813 nm). The bolometric effect induced negative photocurrent is observed among all the three wavelengths with excellent repeatability, which indicates the great potential of integrating ReS_2 transistor in sub-bandgap photodetection and infrared photodetectors. The photoresponse speed of the ReS_2 transistor was also investigated in the infrared regime, as shown in Figure 4c. Both the rising and decaying time are less than 3 ms, exceeding the highest accuracy of our electrical measurement unit. It is worth noting that such photoresponse speed is around 3–4 orders of magnitude faster than that of the previously reported ReS_2 photodetectors.[31,32,36,37] The photoresponsivity (R) of our ReS_2 transistor was also investigated and plotted as a function of wavelength (λ = 800–1200 nm), as shown in Figure 4d. R is defined as the photocurrent generated by per unit power of incident light on the effective area of a photodetector. $R = I_{ph}/(P \cdot S)$, where P is the light intensity, and S is the effective area under illumination. The photoresponsivity shows weak wavelength dependence, with only slight decline from ≈380 to ≈350 AW^{-1} as λ increases from 800 to 1200 nm.

To further illustrate the application of ReS_2 transistor in infrared photodetection, we tested the noise equivalent power (NEP) and specific detectivity (D^*) of the device. **Figure 5**a shows the current noise spectrum of the device at V_g = 50 V, V_{sd} = 0.1 V. It is clear that the 1/f noise dominates in the low frequency regime where f ranges from 1 to 100 Hz, a phenomenon which is also observed at other V_g (Figure S8, Supporting Information). Such 1/f noise is related to the disorder or defects induced fluctuations of local electronic states.[38–40] We then calculated the NEP by using the noise density and photoresponsivity, where NEP = noise density/R. NEP defines the photocurrent signal that is equal to the dark current noise density within 1 Hz bandwidth.[41] The NEP is below 5×10^{-2} pW Hz$^{-1/2}$ over the full infrared spectrum from 800 to 1200 nm (Figure 5b; Figure S9, Supporting Information), indicating the great potential of applying ReS_2 transistor in ultralow light power detection. In addition to NEP, the specific detectivity D^* is also studied. $D^* = (B \cdot S)^{1/2}$/NEP, where B is the measuring bandwidth. Figure 5c shows the D^* as a function of wavelength. The D^* is around 1.3×10^{10} Jones for all wavelengths at V_g = 50 V, which is comparable to that of b-AsP/MoS_2 heterostructure and state-of-the-art PbS based infrared photodetectors in the same spectrum regime at room temperature.[38,41]

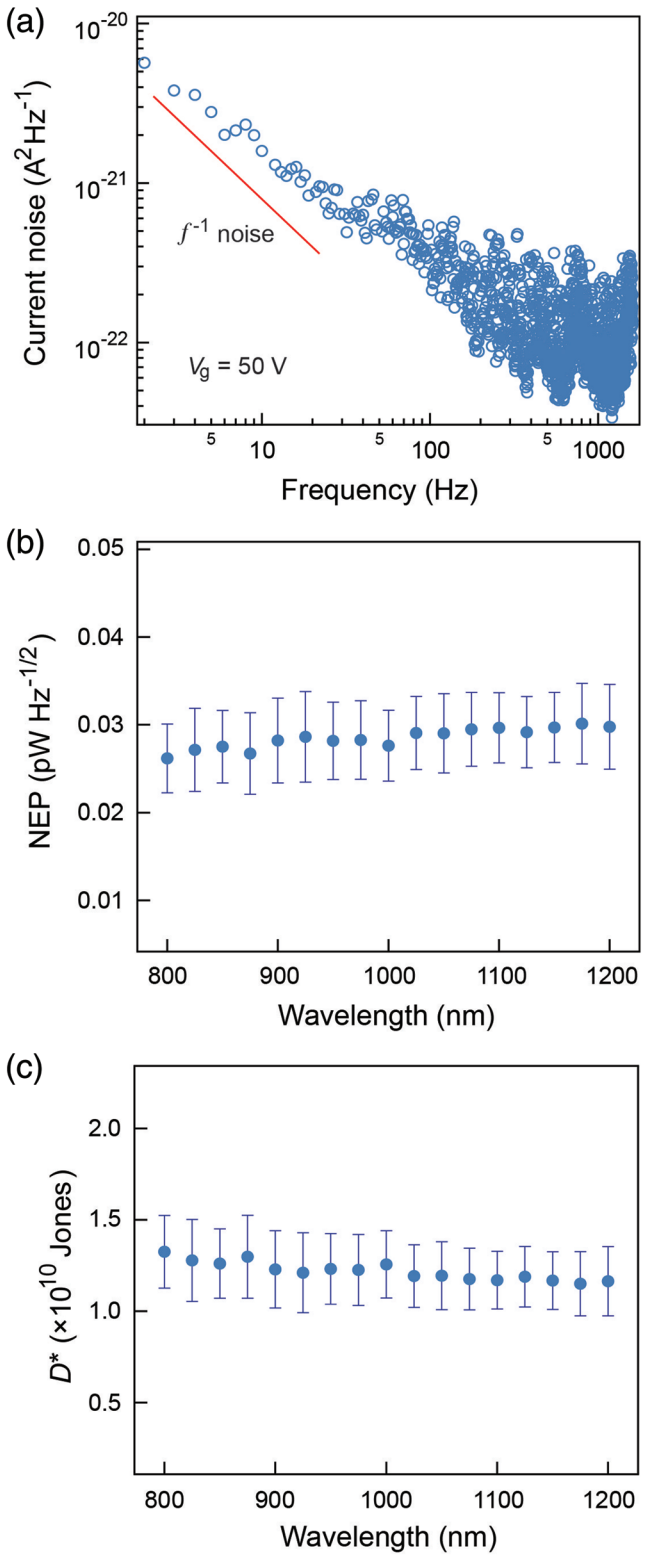

Figure 5. a) Current noise spectrum of the ReS_2 transistor at V_g = 50 V and V_{sd} = 0.1 V. The 1/*f* noise dominates in the low frequency regime. b) The noise equivalent power and c) specific detectivity are plotted as a function of wavelength.

Distinct from the widely studied 2D TMDs such as MoS_2 and WSe_2, ReS_2 possesses a unique distorted 1T phase structure, which enables its anisotropic electrical, optical, and mechanical properties.[34,42] This novel physical degree of freedom is very promising to be applied in 2D logic devices, polarized light photodetectors, and valleytronics. Nevertheless, the anisotropic bolometric effect has not yet been studied in ReS_2, and even among other 2D materials. In the following, we investigated the anisotropic bolometric effect in 2D ReS_2 transistors through angle-resolved photoresponse and transport measurements, as shown in **Figure 6**. Figure 6a exhibits the optical image of the device, in which six pairs of identical metal contacts are deposited on a same ReS_2 flake. Each pair contains two diagonally positioned electrodes with 4 µm channel length, and is spaced evenly by 30°. A fine-focused 638 nm laser with spot diameter around 3 µm was used to illuminate the device center. The gate and bias voltages are fixed at 50 and 0.1 V, respectively, for each photoresponse measurement. Figure 6b shows the angle dependent photocurrent in polar coordinates (Figure S10 of the Supporting Information for detailed photoresponse data). It is to note that the measurements on each pair of contacts include two photocurrents which are spaced by 180° through switching the source–drain current directions. We define that the angle with the lowest photocurrent is 0° (or 180°) for reference. It is obvious that the photocurrent is highly angle dependent, indicating the anisotropic bolometric effect in ReS_2 device. The angle between the highest and the lowest photocurrent is observed as 60° (or 240°), which is in good agreement with the two lattice orientations in ReS_2.[34,42] The anisotropic ratio of the photocurrent $I_{ph}^{max}/I_{ph}^{min}$ is determined to be ≈1.8. To further illustrate the anisotropic bolometric effect, we measured the angle dependent bolometric coefficient β by using the same device with fixed electrode orientation as the photocurrent measurements (Figure 6c). Both the minimum and maximum β are observed in the same direction as the lowest/highest photocurrent. We also calculated the anisotropic ratio of the bolometric coefficient $\beta_{ph}^{max}/\beta_{ph}^{min} \approx 2.0$, which is close to the corresponding photocurrent ratio. The angle-dependent conductance and field effect mobility of another device are also investigated, which show consistent trend with that of the photocurrent and bolometric coefficient (Figure S11, Supporting Information). To understand the effect of light polarization on the anisotropic response, polarized light is used to investigate a two-terminal device (Figure S12, Supporting Information). We observed that the directions of the lowest and highest photocurrent are orthogonal to each other, which is in contrast with the angle-dependence of photocurrent in a circular device. This orthogonality could be attributed to the constant bolometric coefficient in a two-terminal device, leading to a photocurrent that purely determined by the light absorption under different polarization conditions. Therefore, the lattice orientation is of second importance in determining the polarized photocurrent in a two-terminal geometry, while the light polarization condition plays a crucial role. These results further validate the bolometric effect induced photoresponse in our ReS_2 device.

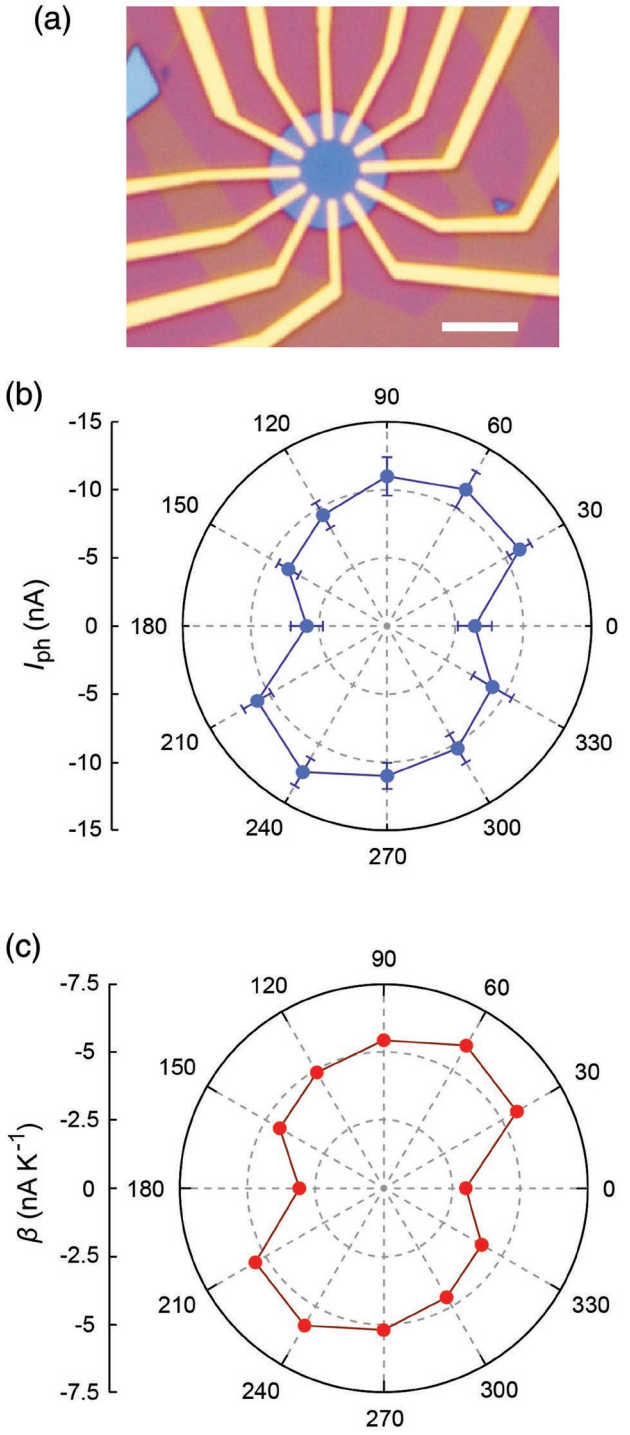

Figure 6. a) Optical image of the ReS_2 device for angle-resolved photoresponse and transport measurements. Six pairs of identical metal contacts are deposited on the ReS_2 flake. Each pair contains two diagonally positioned electrodes with 4 μm channel length, and is spaced evenly by 30°. The scale bar is 5 μm. b) Angle dependent photocurrent and c) bolometric coefficient are plotted in polar coordinates. Note that the measurements on each pair of contacts include two photocurrents which are spaced by 180° through switching the source–drain current direction. The direction with the lowest photocurrent is defined as 0° (or 180°) for reference. The minimum and maximum β are observed in the same direction as the lowest/highest photocurrent.

3. Conclusion

In summary, we have observed bolometric effect induced anomalous photoresponse in ReS_2 transistors with broadband spectrum sensitivity. The photocurrent switches from positive to negative while increasing the backgate under visible light illumination. In addition to visible spectrum, the phototransistor demonstrates significant photoresponse in the infrared regime, where the photon energy is less than the optical bandgap of the ReS_2 flake. The response time is less than 3 ms across the whole wavelength window in the experiments, nearly 3–4 orders of magnitude faster than previously reported ReS_2 photodetectors. Additionally, the phototransistor exhibits a noise equivalent power below 5×10^{-2} pW Hz$^{-1/2}$, and specific detectivity around 1.3×10^{10} Jones over the infrared spectrum, indicating its great potential for ultralow light power detection. Such abnormal photoresponse is also highly anisotropic, which is further supported by the measurement of angle dependent bolometric coefficient. Our observations shed new light onto the broadband photodetection in large bandgap TMDs-based photodetectors, and open up new opportunities in integrating these materials in the all-spectrum light-sensing applications.

4. Experimental Section

Sample Preparation and Device Fabrication: The ReS_2 flakes were mechanically exfoliated from bulk ReS_2 crystals (HQ graphene) using a scotch tape and transferred onto degenerately p-type doped silicon wafers coated with 300 nm SiO_2. The exfoliated ReS_2 flakes were located by using high resolution microscope (Nikon Eclipse LV100D) followed by the spin-coat of photoresist PMMA. The source and the drain electrodes were patterned on the flake using the conventional e-beam lithography technique. After lithography, metal electrodes Ti (5 nm) and Au (80 nm) were thermally deposited on the flakes in high vacuum (≈10^{-7} mbar). The devices were then liftoff in acetone solution. After liftoff, the as-made devices were wire-bonded onto an LCC chip carrier and loaded in a custom designed high vacuum system (≈10^{-8} mbar) for electrical and optoelectrical measurements.

Device Characterization: The electrical and optoelectrical measurements were conducted by using an Agilent 2912A source measure unit. Three laser beams (638, 515, 473 nm) and an exon light source configured with a monochromator were used to illuminate the device. Note that the spot size of xenon light is around 20 mm^2. For the anisotropic photoresponse measurement, the laser beam was focused on the device center by using a 50× objective lens. The light density was calibrated by THORLABS GmbH (PM 100A) power meter. To acquire the noise spectra, the source terminal of the ReS_2 transistor was DC coupled to Stanford Research SR570 low noise current preamplifier. The output of this current amplifier was recorded by an HP 35670A dynamic signal analyzer. The frequency ranges from 1 to 1600 Hz for each noise spectrum measurement.

Supporting Information

Supporting Information is available from the Wiley Online Library or from the author.

Acknowledgements

D.X. and T.L. contributed equally to this work. The authors acknowledge the financial support from Natural Science Foundation of China

(21573156 and 21872100), Natural Science Foundation of Jiangsu Province under Grant No. BK20170005, and Singapore MOE Grants of R143-000-652-112 and R143-000-A43-114 and NUS TAP grant of R143-000-A98-118. D.X. acknowledges Dr. W. Liao for the assistance in the noise measurement.

Conflict of Interest

The authors declare no conflict of interest.

Keywords

2D ReS_2 transistors, bolometric modes, low noise equivalent power, fast photoresponse, photocurrent polarity switching, sub-bandgap photodetection

Received: July 2, 2019
Revised: September 17, 2019
Published online:

[1] D. L. Mathine, *IEEE J. Sel. Top. Quantum Electron.* **1997**, *3*, 952.
[2] R. Soref, *IEEE J. Sel. Top. Quantum Electron.* **2006**, *12*, 1678.
[3] L. Tsybeskov, D. J. Lockwood, M. Ichikawa, *Proc. IEEE* **2009**, *97*, 1161.
[4] K. F. Mak, J. Shan, *Nat. Photonics* **2016**, *10*, 216.
[5] F. H. L. Koppens, T. Mueller, P. Avouris, A. C. Ferrari, M. S. Vitiello, M. Polini, *Nat. Nanotechnol.* **2014**, *9*, 780.
[6] M. Long, P. Wang, H. Fang, W. Hu, *Adv. Funct. Mater.* **2018**, *29*, 1803807.
[7] D. Xiang, T. Liu, J. Xu, J. Y. Tan, Z. Hu, B. Lei, Y. Zheng, J. Wu, A. H. C. Neto, L. Liu, W. Chen, *Nat. Commun.* **2018**, *9*, 2966.
[8] T. Liu, D. Xiang, Y. Zheng, Y. Wang, X. Wang, L. Wang, J. He, L. Liu, W. Chen, *Adv. Mater.* **2018**, *30*, 1804470.
[9] Y. Chen, Z. Fan, Z. Zhang, W. Niu, C. Li, N. Yang, B. Chen, H. Zhang, *Chem. Rev.* **2018**, *118*, 6409.
[10] F. Xia, H. Wang, D. Xiao, M. Dubey, A. Ramasubramaniam, *Nat. Photonics* **2014**, *8*, 899.
[11] Y. Venkata Subbaiah, K. Saji, A. Tiwari, *Adv. Funct. Mater.* **2016**, *26*, 2046.
[12] K. Novoselov, A. Mishchenko, A. Carvalho, A. C. Neto, *Science* **2016**, *353*, aac9439.
[13] D. Geng, H. Y. Yang, *Adv. Mater.* **2018**, *30*, 1800865.
[14] M. Freitag, T. Low, F. Xia, P. Avouris, *Nat. Photonics* **2013**, *7*, 53.
[15] X. Gan, R.-J. Shiue, Y. Gao, I. Meric, T. F. Heinz, K. Shepard, J. Hone, S. Assefa, D. Englund, *Nat. Photonics* **2013**, *7*, 883.
[16] T. Mueller, F. Xia, P. Avouris, *Nat. Photonics* **2010**, *4*, 297.
[17] F. Xia, T. Mueller, Y.-m. Lin, A. Valdes-Garcia, P. Avouris, *Nat. Nanotechnol.* **2009**, *4*, 839.
[18] Q. Guo, A. Pospischil, M. Bhuiyan, H. Jiang, H. Tian, D. Farmer, B. Deng, C. Li, S.-J. Han, H. Wang, Q. Xia, T.-P. Ma, T. Mueller, F. Xia, *Nano Lett.* **2016**, *16*, 4648.
[19] N. Youngblood, C. Chen, S. J. Koester, M. Li, *Nat. Photonics* **2015**, *9*, 247.
[20] D. Xiang, C. Han, J. Wu, S. Zhong, Y. Liu, J. Lin, X.-A. Zhang, W. Ping Hu, B. Özyilmaz, A. H. C. Neto, A. T. S. Wee, W. Chen, *Nat. Commun.* **2015**, *6*, 6485.
[21] H. Liu, Y. Du, Y. Deng, P. D. Ye, *Chem. Soc. Rev.* **2015**, *44*, 2732.
[22] J. Wu, G. K. W. Koon, D. Xiang, C. Han, C. T. Toh, E. S. Kulkarni, I. Verzhbitskiy, A. Carvalho, A. S. Rodin, S. P. Koenig, G. Eda, W. Chen, A. H. C. Neto, B. Özyilmaz, *ACS Nano* **2015**, *9*, 8070.
[23] Z. Yin, H. Li, H. Li, L. Jiang, Y. Shi, Y. Sun, G. Lu, Q. Zhang, X. Chen, H. Zhang, *ACS Nano* **2012**, *6*, 74.
[24] O. Lopez-Sanchez, D. Lembke, M. Kayci, A. Radenovic, A. Kis, *Nat. Nanotechnol.* **2013**, *8*, 497.
[25] C. Xie, C. Mak, X. Tao, F. Yan, *Adv. Funct. Mater.* **2017**, *27*, 1603886.
[26] J.-Y. Wu, Y. T. Chun, S. Li, T. Zhang, J. Wang, P. K. Shrestha, D. Chu, *Adv. Mater.* **2018**, *30*, 1705880.
[27] F. Cui, C. Wang, X. Li, G. Wang, K. Liu, Z. Yang, Q. Feng, X. Liang, Z. Zhang, S. Liu, Z. Lei, Z. Liu, H. Xu, J. Zhang, *Adv. Mater.* **2016**, *28*, 5019.
[28] X. He, F. Liu, P. Hu, W. Fu, X. Wang, Q. Zeng, W. Zhao, Z. Liu, *Small* **2015**, *11*, 5423.
[29] M. Rahman, K. Davey, S.-Z. Qiao, *Adv. Funct. Mater.* **2017**, *27*, 1606129.
[30] Q. Zhang, S. Tan, R. G. Mendes, Z. Sun, Y. Chen, X. Kong, Y. Xue, M. H. Rümmeli, X. Wu, S. Chen, L. Fu, *Adv. Mater.* **2016**, *28*, 2616.
[31] E. Zhang, Y. Jin, X. Yuan, W. Wang, C. Zhang, L. Tang, S. Liu, P. Zhou, W. Hu, F. Xiu, *Adv. Funct. Mater.* **2015**, *25*, 4076.
[32] F. Liu, S. Zheng, X. He, A. Chaturvedi, J. He, W. L. Chow, T. R. Mion, X. Wang, J. Zhou, Q. Fu, H. J. Fan, B. K. Tay, L. Song, R.-H. He, C. Kloc, P. M. Ajayan, Z. Liu, *Adv. Funct. Mater.* **2016**, *26*, 1169.
[33] S. Tongay, H. Sahin, C. Ko, A. Luce, W. Fan, K. Liu, J. Zhou, Y.-S. Huang, C.-H. Ho, J. Yan, D. F. Ogletree, S. Aloni, J. Ji, S. Li, J. Li, F. M. Peeters, J. Wu, *Nat. Commun.* **2014**, *5*, 3252.
[34] E. Liu, Y. Fu, Y. Wang, Y. Feng, H. Liu, X. Wan, W. Zhou, B. Wang, L. Shao, C.-H. Ho, Y.-S. Huang, Z. Cao, L. Wang, A. Li, J. Zeng, F. Song, X. Wang, Y. Shi, H. Yuan, H. Y. Hwang, Y. Cui, F. Miao, D. Xing, *Nat. Commun.* **2015**, *6*, 6991.
[35] A. Allain, J. Kang, K. Banerjee, A. Kis, *Nat. Mater.* **2015**, *14*, 1195.
[36] J. Shim, A. Oh, D.-H. Kang, S. Oh, S. K. Jang, J. Jeon, M. H. Jeon, M. Kim, C. Choi, J. Lee, S. Lee, G. Y. Yeom, Y. J. Song, J.-H. Park, *Adv. Mater.* **2016**, *28*, 6985.
[37] E. Liu, M. Long, J. Zeng, W. Luo, Y. Wang, Y. Pan, W. Zhou, B. Wang, W. Hu, Z. Ni, Y. You, X. Zhang, S. Qin, Y. Shi, K. Watanabe, T. Taniguchi, H. Yuan, H. Y. Hwang, Y. Cui, F. Miao, D. Xing, *Adv. Funct. Mater.* **2016**, *26*, 1938.
[38] M. Long, A. Gao, P. Wang, H. Xia, C. Ott, C. Pan, Y. Fu, E. Liu, X. Chen, W. Lu, T. Nilges, J. Xu, X. Wang, W. Hu, F. Miao, *Sci. Adv.* **2017**, *3*, e1700589.
[39] A. A. Balandin, *Nat. Nanotechnol.* **2013**, *8*, 549.
[40] J. Na, Y. T. Lee, J. A. Lim, D. K. Hwang, G.-T. Kim, W. K. Choi, Y.-W. Song, *ACS Nano* **2014**, *8*, 11753.
[41] L. Wang, L. Huang, W. C. Tan, X. Feng, L. Chen, K.-W. Ang, *Nanoscale* **2018**, *10*, 14359.
[42] Y.-C. Lin, H.-P. Komsa, C.-H. Yeh, T. Björkman, Z.-Y. Liang, C.-H. Ho, Y.-S. Huang, P.-W. Chiu, A. V. Krasheninnikov, K. Suenaga, *ACS Nano* **2015**, *9*, 11249.

